Curvature sensing with a spherical tactile sensor using the color-interference of a marker array

Xi Lin[1,2], Laurence Willemet[1], Alexandre Bailleul[1] and Michaël Wiertlewski[2]

***Abstract*— The only way to perceive a small object held between our fingers is to trust our sense of touch. Touch provides cues about the state of the contact even if its view is occluded by the finger. The interaction between the soft fingers and the surface reveals crucial information, such as the local shape of the object, that plays a central role in fine manipulation. In this work, we present a new spherical sensor that endows robots with a fine distributed sense of touch. This sensor is an evolution of our distributed tactile sensor that measures the dense 3-dimensional displacement field of an elastic membrane, using the subtractive color-mixing principle. We leverage a planar manufacturing process that enables the design and manufacturing of the functional features on a flat surface. The flat functional panels are then folded to create a spherical shape able to sense a wide variety of objects.**

The resulting 40mm-diameter spherical sensor has 77 measurement points, each of which gives an estimation of the local 3d displacement, normal and tangential to the surface. Each marker is built around 2 sets of colored patches placed at different depths. The relative motion and resulting hue of each marker, easily captured by an embedded RGB camera, provides a measurement of their 3d motion. To benchmark the sensor, we compared the measurements obtained while pressing the sensor on a curved surface with Hertz contact theory, a hallmark of contact mechanics. While the mechanics did strictly follow Hertz contact theory, using the shear and normal sensing, ChromaTouch can estimate the curvature of an object after a millimeter-size indentation of the sensor.

I. Introduction

Robots interact with their surroundings by sensing and reacting to the mechanical behavior of the environment, usually through an impedance control feedback loop [1]. In a classical impedance control, the mechanical interaction with the environment is measured with a force sensor and serves as a basis to control the motion of the robotic arm at modulating its apparent stiffness. Yet, perceiving the mechanical world with only a single point of measurement discards the abundance of information that the mechanical scene has to offer. A single 6-axis force sensor can indeed be used to find the timing, location, and direction of a contact force [2], [3] but the limited spatial distribution of the data prevents the estimation of the shape and the surface properties of an object without active exploration [4].

Humans also use proprioception to gather kinematic information to control the impedance of their limbs, but what set them apart is that they are endowed with a rich sense of touch, mediated by a collection of mechanoreceptors, densely populated in the fingertips. This wide-ranging array of mechanoreceptors encodes the complex mechanical interaction that occurs at the contact between the skin and the object. The sense of touch captures surface features [5], [6], compliance of materials [7], [8] or the presence of edges [9]. Of importance for the present work, an estimate of the curvature of an object can be extracted from a single press [10] and guide the timing of motor commands required for grasping and object manipulation [11], [12].

Given the usefulness of touch in manipulation, it is not surprising that tactile sensors for robotics have shown great promise in providing a rich image of the mechanical interaction on a par with human perception. A large variety of strategies can be used to transduce the mechanical deformation into an electrical signal, for a full review the reader can refer to [13]. Amongst these techniques, camera-based tactile sensors attract increasing attention due to their higher spatial resolution and minimum wiring requirement compared to other tactile sensing technologies. These sensors typically use a camera to track the displacements of markers embedded in a soft elastomer. This method delivers dense tactile images with a relatively fine temporal resolution when leveraging high frame-rate cameras [14], [15]. However, except for a few exceptions detailed in the next section, these sensors usually are limited to measuring lateral deformation, which provides valuable measurements but requires complex processing and approximations to gauge the normal motion of each marker.

The ChromaTouch sensor, introduced in [16], solves the

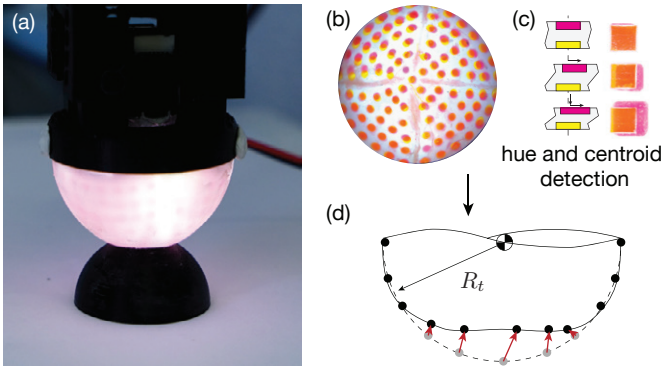

Fig. 1. (a) The sensor, mounted on a robotic arm, explores an object (b) Typical image retrieved by the embedded camera (c) Effect of lateral and normal forces on the shape and hue of a marker. (d) After calibration, the lateral and normal deformation of each point is estimated.

This work was supported by *Agence Nationale de la Recherche* within the PHASE project 16-CE10-0003

[1]Xi Lin, Laurence Willemet and Alexandre Bailleul are with ISM, CNRS and Aix-Marseille Université, France {name.surname}@univ-amu.fr

[2]Michael Wiertlewski is with the Cognitive Robotics Department of TU Delft, Netherlands m.wiertlewski@tudelft.nl

problem by encoding the normal motion of each marker in the color channels of the camera, effectively converting a 2-dimensional color image information into 3-dimensional deformation field. Each marker is made by 2 overlapping submarkers, one diffusive and magenta, the other translucent and yellow. The full 3d relative motion of the submarkers is found from both the centroid detection and the change of hue of the marker. We demonstrated the effectiveness of this transduction principle to detect dense 3d displacement fields on a flat sensing surface. The long-term goal of the work is to integrate this sensor in with a robotic end-effector with curved fingertips. In this paper, we introduce a new version of ChromaTouch that uses the color-mixing transduction principle on a hemispherical sensing surface, able to explore surfaces with arbitrary shapes, see 1a. The sensor embeds a camera equipped with a fisheye lens, which has the double benefit of amplifying the signal used to estimate the normal displacements as well as unwrapping the spherical projection of the sensing hemisphere, see 1b. Figure 1c, illustrates the sensing method. After calibration, the sensor retrieves the 3d deformation field at the location of the markers which can be interpolated into the full deformation of the body, see fig 1d.

II. Related work

A. Camera-based sensors

The success of camera-based tactile sensors can be attributed to the decades of engineering that refined camera sensors and allowed converting photons into digital data. By relying on off-the-shelf camera, these sensors bypass the electronic engineering that is required to make capacitive and piezo-resistive tactile sensors. For this reason, camera-based sensors often boast larger resolution and higher refresh-rate.

Camera-based tactile sensors rely on a deformable medium seen by the camera, which essentially converts the mechanical interaction into a visible change of the image. Therefore, the necessary inventiveness to extract data about the contact lies in the engineering of this medium. The simplest method is to place black markers on a white background on a soft elastomer and track the motion of these markers to infer the interaction at the contact. The biomimetic approaches suggest amplifying motion via an array of pins attached to a deformable membrane [19]. However, the transduction from the 2D optical image to a 3D mechanical deformation field remains a challenge [17], mainly because the distance from the markers to the camera is unknown.

GelForce developed by [14] employing double layers of rigid markers to compute the 3D stress field. The normal stresses are calculated from the lateral distribution of the markers. This implementation is effective but the spatial resolution of the sensor is limited, because the markers on both layers cannot be overlaid. The GelSight sensor measures the topography of an elastomer covered by a light-reflecting membrane illuminated from 3 sides by 3 lights of complementary color. The 3d geometry of the deformation of the gel is reconstructed from the shadow of the asperities in contact with the membrane. The sensor has been used with added markers to measure the slip and shear at the contact [20], [15]. Because of its working principle, these sensors can only be planar or have small curvature, and therefore accommodate well only with convex objects. In [18], the tactile sensor uses the change of color to determine normal pressure with 3×3 markers.

The ChromaTouch sensor builds upon these principles and extends to the recovery of the full displacement field to gather a complete picture of the contact.

B. Spherical-shaped sensors

Soft spherical-cap artificial fingertips are popular in robotic grasping as they help stabilizing the contact with an arbitrarily shaped object. Therefore, a large body of research has created artificial fingertips with spherical or complex convex shapes.

A wide array of manufacturing strategies has been deployed. Casting the body of the sensor in a spherical mold, with grooves results in structures with soft and complex shape that can even incorporate markers if the grooves are included in the mold [21]. Another popular fabrication method makes use of 3d printing with soft elastomer. 3d printing offers a versatile method for producing complex-shaped sensors [19]. One of the downside of spherical sensors has to do with the fact that circular markers on a sphere will appear as ellipses when projected on the image plane. Several sensors subsequently require image wrapping to recover the proper shape of markers [21].

Alternatively, piezoresistive and capacitive sensors can be mounted on a flexible printed circuit board that is cut and wrapped around a rigid core, then covered with a rigid layer [22]. The cover filters and blurs the signal from the contact thus markers benefit from being near to the surface [23].

III. Convex sensor to measure convex and concave objects

A. The case for spherical shape when exploring objects

Simple reasoning can highlight why a curved sensor is beneficial for the versatility of sensing with arbitrary objects.

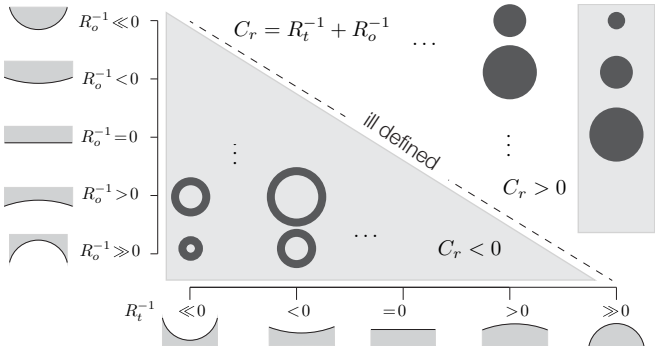

Fig. 2. Shape of the contact between a sensor with curvature R_t^{-1} and an object with curvature R_o^{-1}. When relative curvature C_r is null, the contact topology is ill-defined. Since the environment of the robot contains objects of undefined curvatures, a small radius will provide the best versatility. The shaded area shows the operating range of curvature that spherical sensors can typically sample.

It allows the sensor tip to conform to the touched object with a larger contacting surface [24], [25]. The shape and size of the contact surface are determined by the relative curvature at the contact point. Assuming concave or convex spherical sensor and object, the relative curvature can be expressed as $C_r = R_t^{-1} + R_o^{-1}$, where R_t is the radius of the sensor, and R_o is the local radius of the object, near the contact point. The radius is positive for the convex object and negative for the concave object. When the object is flat, the radius is infinite and the curvature of the object is null. If both the sensor and the objects are flat, the relative curvature is null, and in this special case, the contact is made on the higher asperities of both surfaces, therefore, relying on stochastic properties and being ill-defined at macroscopic scales [26].

On the other hand, when the relative curvature is negative — the concave object has a smaller radius than the convex object — the contact is made at the edge of the convex object and therefore the mechanical interaction is discontinuous. From a sampling point of view, in order to have an uninterrupted contact surface, the best choice is to have positive relative curvature (see Figure 2). In this case, the contact follows Hertz theory and the contact area is elliptical.

This result is well known by the mechanical community and is the reason why surface scanning instruments have small diameter tips and can capture the small-scale changes in curvature [26].

B. Flat to curved projection

The manufacturing of the double overplayed layer needed for ChromaTouch requires the alignment of magenta and yellow dots on two different planes. This sensitive operation is relatively straightforward to process on flat surface but challenging when the alignment must be done on a curved surface, such as a sphere.

Gauss' *Theorema Egregium* provides an opportune framework to understand how to design a flat part that can be folded. The remarkable theorem states that the Gaussian curvature κ — defined by being the product of each principal curvature — of a surface is invariant under bending. A flat plane of Gaussian curvature $\kappa = 0$ can be bent along one dimension for which one of the principal curvatures will be non-zero, but cannot be deformed into a sphere for which both principal curvatures will be the reciprocal of the bending radius R_b, i.e. $\kappa = 1/R_b^2$. Since bending and folding are not sufficient to make the sphere, in our production process, the surface has to be stretched or cut.

To work out a way around this fundamental constraint, we used a production method that is popular for making spherical globes from flat maps. The sphere is divided into n gores (i.e. segments), each of which can be worked on as it is a flat surface. In globe production, each of the gore contains a part of the map so that the shape and linearity of the meridian are preserved. Once the gores are printed, they are folded into a sphere to make the globe. The fold introduced a small distortion as the flat gores still must be bent in both directions. However, as the number of gores increases, the bend along the equator is less pronounced and the distortion induced by stretch is reduced. In our case, because we are using compliant elastomers which forgive some stretch, cutting the sphere in 4 gores was enough to ensure an easy manufacturing process, while reducing the number of seams.

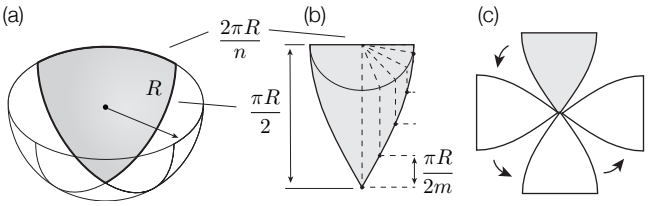

Fig. 3. Construction of the polyconic pattern. (a) One of the n^{th} segment — called gore — of the sphere (b) is constructed by projecting m regularly spaced points of an inner circle whose diameter is the equator of a segment onto a regular line grid spaced by $\pi R/2m$ (c) The segment is then copied n times and rotated around its apex to produce the final flat pattern.

Figure 3 illustrates the process used to create the shape of the gores and assemble them into a spherical cap of radius R. The shape of each gore is found by constructing a semicircle with a diameter the equatorial edge of length $2\pi R/n$. Then we divide the inner circle in m radii and project the vector field onto a regularly spaced grid of which extend from the equator line to a parallel line spaced by $\pi R/2$. Placing the markers onto the flat gores is effortless compared to assembling them on a spherical surface. Regular manufacturing techniques such as printing, laser cutting, molding can be used to create the required pattern.

C. Manufacturing process

The manufacturing process illustrated in figure 4 is an update from the original flat version [16]. First, the base is cast from transparent elastomer (Sortaclear 12, Smooth-On, Macungie, PA, USA) in a high-resolution 3d-printed mold. The grooves left by the cast are filled with the magenta markers, made from the same elastomer in which a dye is added. Then, a protective layer is molded, on top of which the yellow filter is placed. The yellow elements are laser cut and the rest of the film are discarded. A protective transparent layer embeds the yellow transparent submarkers. The whole operation including curing takes approximately 2 days.

At this stage, the manufacturing process requiring the part to be flat are completed and the pattern is folded onto a rigid and transparent sphere made of acrylic. Lastly, the white outer layer is cast onto the exterior of the sphere to ensure the proper cohesion of the gores. The last external layer also acts as a barrier for external light and as a diffuser for the marker illumination.

D. Assembly and optical image correction

Within the current limit of our off-the-shelf manufacturing process, we can create spherical sensors with 77 markers measuring 2 mm in diameter and distributed on the meridians of a sphere of radius 40 mm. A USB-camera (Aria A15S-C, Alkeria, Cascina, Italy), with a 1/2.9" image sensor, is placed at the center of the sphere. The camera is fixed onto a mounting fixture that is linked to the force sensor of the

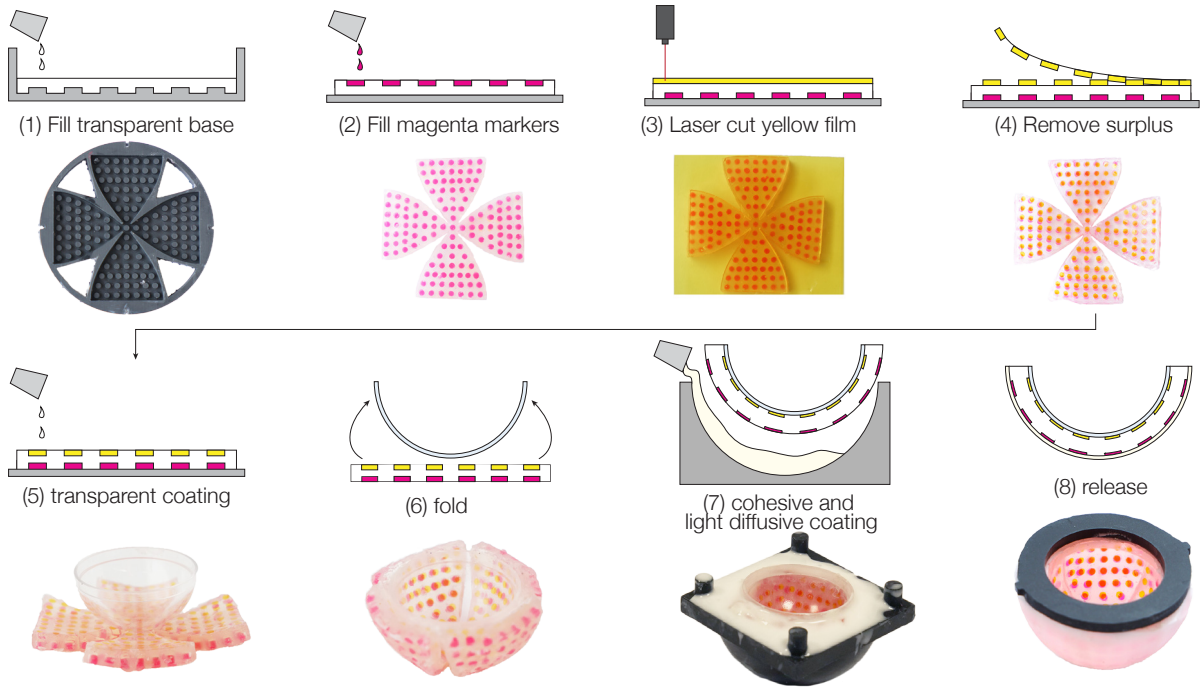

Fig. 4. Manufacturing process. A flat mold makes alignment of the magenta and yellow marker easier. Once the flat pattern is completed, it is folded into a spherical shape, and held in place by curing additional elastomer, which acts as a diffuser for the illumination.

robot arm. The overall assembly of the sensor is shown in figure 5a.

The camera is equipped with a f = 2.2 mm fisheye wide lens (Lensagon BF5M2223S129, Lensation GmbH, Karlsruhe, Germany). As found previously [16], the interference of the marker is most notable when the lens has a short focal length, which provides a better signal to noise ratio. The fisheye lens has a 180° field of view, which usually creates a characteristic distortion due to the equidistant projection. However, in this case, each marker is at the same distance from the focal of the lens and cancels exactly the distortion made by projecting the markers onto a plane. The image created by the combination of the fisheye lens and spherical marker array creates an image without needing post-processing for image distortion.

E. Signal processing

The 3-dimensional displacement of each marker with respect to the camera depends on the observed lateral displacement of the centroid and the change of hue of their projection on the image sensor. To convert the image into a vector field, a processing pipeline is as follows. First, the raw images from the camera are cropped using a circular mask to remove everything outside of the edge of the sensor. Then a *tophat* filter is applied to mitigate the effect of non-uniform lighting and the contrast is enhanced. Once the correction is done, the images are converted from RGB to HSV color space. The hue channel is used to segment the markers by thresholding around the yellow and magenta hue. The centroid of each magenta marker is detected from the binary images using the *regionprop* function in Matlab. The mask

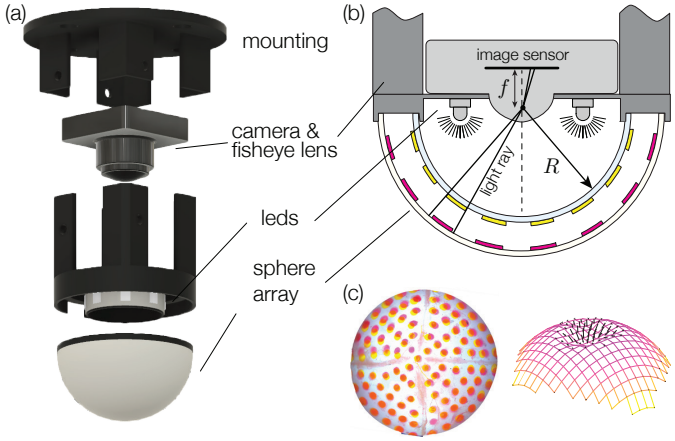

Fig. 5. (a) Exploded view of the assembly. (b) The fisheye lens creates a flat projection of the spherical array, canceling the distortions. The markers have similar area throughout the image. (c) The resulting image and estimation of the local shape and deformation.

is used to isolate the marker in the original image. For each marker, the average hue is stored. At this stage, we have the hue, which reflects the normal displacement, and the motion of the centroid in 2 dimensions, which reflects the lateral displacement of the markers.

IV. Experimental validation

A. Calibration

The link between the hue of the marker and the actual displacement it experiences is influenced by the construction, illumination, and camera parameters. Therefore, this relationship needs to be calibrated against a ground truth.

The calibration is done by pressing the sensor onto a flat plate, with a robot (UR3, Universal Robots, Odense, Denmark) equipped with a force-torque sensor (FT300, Robotiq, Lévis, Canada) to measure interaction forces. During a normal loading experiment, the force and the displacement of the robot are recorded to provide ground truth for the load curve of the system. At the same time, the state of each marker is determined to find the distribution of the displacement over the contact area.

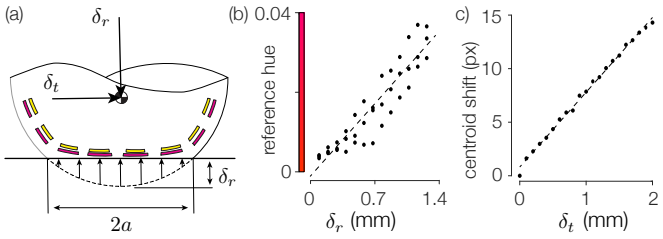

Fig. 6. (a) Effect of pressing the spherical sensor on a plane (b) The reference hue as a function of the normal displacement of the robotic arm, and its linear fit in dashed line. (c) Results from the tangential calibration.

As shown in figure 6a, the external force P applied by the robot will induce a deformation δ_r of the soft sensor if the contacting surface is infinitely stiff compared to the compliance of the soft elastomer of the sensor. This deformation δ_r also corresponds to the maximum of the deformation field measured by the tactile sensors, independently of the curvature of the object. Therefore, we can use the ground truth values to calibrate the variation of observed hue.

Figure 6b, shows typical traces obtained during calibration. The relationship between the hue of the marker that experiences the maximum deformation (i.e. located in the center of the contact patch) and the displacement recorded by the robot is invariant with the curvature of the contacting object. A linear fit gives the coefficient to extrapolate the displacement from any arbitrary observed hue. The goodness of fit on the sampled data is $R^2 = 0.89$. A similar procedure is done for the lateral displacement with the goodness of fit $R^2 = 0.99$, see figure 6c.

B. Example application: model-driven curvature estimation

Once the relationship between the observed hue and the displacement is established, we can reconstruct the 3d displacement field of the sensor from the observed images sampled at the location of the markers. The data is then interpolated again to provide a regularly spaced sampling.

The contacts with two curved objects of radii ± 80 mm and a flat surface are illustrated in figure 7. The image reveals a difference in the extent to which the markers are disturbed. The measured displacement field reveals the nature of the interaction. The field shows a peak at the center of the contact that tapers as the edge of the contact in a monotonic fashion. It is interesting to note that the local contact force is not strictly normal to the surface but has a slight angle due to the work of friction and elastic stretch. The measurement of the lateral motion has importance in evaluating the shape of the normal deformation since the markers moved. The red dots in Fig 7 show the normal displacement at the original radial location of the markers.

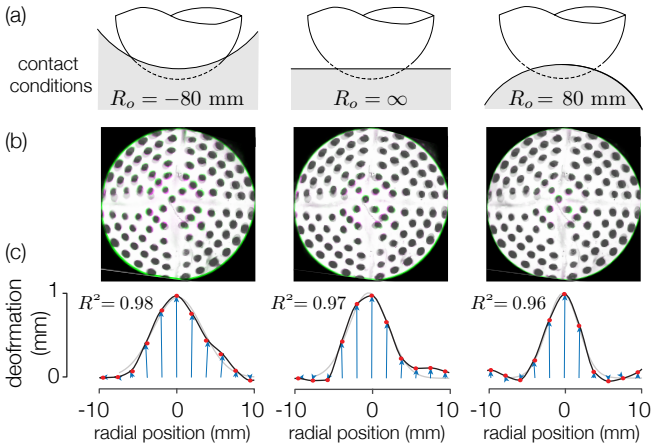

Fig. 7. (a) Comparison between Hertz contact theory and measurement given by the sensor when pressing on a negative, null and positive curvature object. (b) The image difference between the normal state and the deformed state is affected by the curvature of the object. The negative difference is in magenta and the positive in green. (c) The resulting profile of the displacement of the middle cross-section of markers. The vectors show the actual displacement of each marker, the red dots highlight only the normal motion and the gray curves show the result of curve-fitting with a filtered Hertzian contact.

The Hertz contact theory can be used to analyze the measured displacement and extract the radius of the contacting body [27]. In the following paragraph, the assumption is that the object is infinitely rigid compared to the soft fingertip. The theory first observes that the contact area between two spherical objects will lead to a circular contact area of radius a. The relative displacement of the two bodies δ_r is related to the contact area a^2 by the equivalent radius $R = (R_s^{-1} + R_o^{-1})^{-1}$ such as:

$$a^2 = R\delta_r \tag{1}$$

where the effective radius is calculated with the radius of the sensor R_s and the radius of the object R_o in contact. This equation can be reversed to find the radius of the object from the displacement and the area of contact, knowing the radius of the object.

According to Hertz theory, the contact at the surface should lead to normal displacement u_z of the soft body which follows a parabolic shape such as:

$$u_z(r)|_{z=0} = \delta_r \left(1 - \frac{r^2}{a^2}\right) \tag{2}$$

where r is the radial coordinate. Curve fitting this relationship to the measurement, could in theory resolve from tactile data the displacement of the sensor and the area of the contact patch. However, the measured displacements from ChromaTouch come from the markers that are embedded deeper in the elastomer. The elastomeric layer that covers the markers acts as a mechanical filter and blurs the contact distribution. In order to simplify the fitting procedure, the distribution is approximated by a gaussian curve

$u_z(r)|_{z=2\text{mm}} = \delta_r \exp\left(-r^2/2a^2\right)$, from which the amplitude is the global displacement and the deviation is related to the area of contact. Figure 8a illustrates the filtering done by the soft tissues, which can be estimated from Boussinesq-Cerruti equations. The gaussian approximation has a goodness of fit with the theoretical deformation of $R^2 = 0.96$.

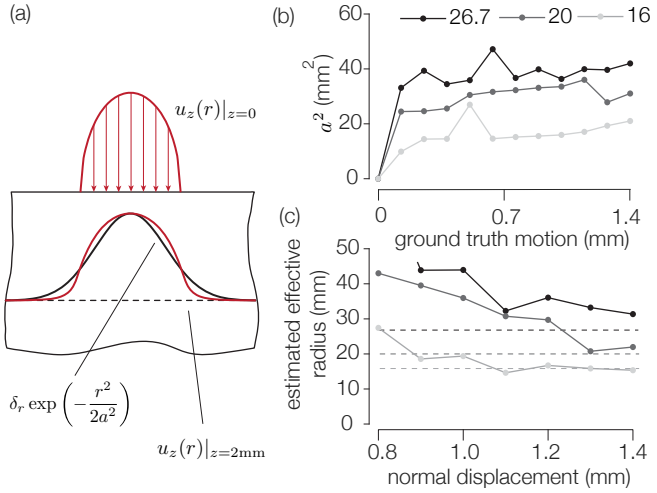

Fig. 8. (a) Sensors embedded in the elastomer inherently observe a blurry picture of the contact. (b) Evolution of the contact area as the sensor is pushed into a curved object. (b) Results of the estimation of the curvature at the beginning of the press. The estimated effective radius (plain lines) converge to the real value (dashed lines).

We conducted measurements on three spherical objects mentioned earlier. Figure 8b shows the estimation of the area of contact a^2 extracted from the gaussian fit, when the normal displacement of the robot increases. The radius of the contact area increases with the applied normal displacement. The equivalent curvature is computed from the deformation field. Figure 8c reveals that the equivalent curvature converges to the actual curvature when the normal displacement increases, although some discrepancies exist. For indentation lower than a millimeter, the noise of measurement has a significant influence on the quality of results. After a normal displacement of 1 mm, the estimation converges to the real value. When the total displacement reaches 1.4 mm, the estimations of the effective radius R corresponds well the desired values, which are $R = \{26.7\text{mm}, 20\text{mm}, 16\text{mm}\}$ for the sensor with the radius of $R_t = 20$ mm in contact with objects with the radius of $R_o = \{-80\text{mm}, \infty, 80\text{mm}\}$ respectively.

V. Discussion and Conclusions

A. Discussion

Tactile sensors are essential tools to enable robots to haptically explore their surroundings, perceive changes in contact conditions and subsequently accomplish dexterous manipulation tasks. The spherical shape associated with the use of soft elastomer offers tactile sensing as well as intrinsic stability when grasping. The color subtraction method, presented in this work, enables access to the shear as well as the normal components of the deformation, which is theoretically enough to reconstruct the stress pattern at the surface. The current work shows that the deformation of the sensor is in good agreement with the Hertz contact theory despite showing some striking differences.

During the experiment, we made sure that the contact was lubricated, therefore as close to frictionless as possible, to follow the assumptions underlying Hertz contact theory. Upon contact, the section touching the object expanded laterally to maintain its surface area. The displacement of individual points did not follow a pure normal path but was also shifted toward the outside of the contact patch contrary to the prediction of Hertz theory in which the displacement is purely normal. The discrepancy with the linear small-strain theory of Hertz is most certainly due to large deformations of the soft layers of the sensor. The lateral motion could be used to estimate slipperiness of the surface without having to slide the sensor laterally. Some evidence shows similar capabilities of friction perception while pressing in humans [28], [29].

Lastly, the lateral calibration is performed only at one normal force, but it appears to be affected by the indentation depth, which translates into an underestimation. Finer calibration procedure should lead to even more accurate results.

B. Future improvements

The analysis of the experimental results suggests several essential improvements. First of all, the rigid core inside the sensor should be removed to have a more linear deformation pattern and to avoid saturation of the sensor at higher loads. Along those lines, future sensors will use a softer compound to maximize the deformation and color changes of the markers inside the sensor.

Second, in this study, the sphere was made using four gores which is practical from the standpoint of folding but still induces too much stress and distortion when wrapped around the spherical core. The sweet spot between low distortion and ease of manufacturing might be closer to 6 or 8 gores. Increasing the number of markers to provide better spatial resolution will offer the possibility of digital spatial filtering that can improve the signal to noise ratio.

Lastly, the calibration procedure will be replaced by a machine-learning approach in the hope that it considers the deviation from the calibration of each marker.

C. Conclusion

This work presents a new hemispherical version of the camera-based tactile sensor developed by [16]. The sensor can measure the 3d deformation field of the contact via marker tracking and hue detection. With the hemispherical configuration, the sensor is suited to explore surfaces with arbitrary curvature even if the object is slightly concave. We proposed an algorithm to estimate the curvature of the object with a 1 mm indentation on the object. Experimental results show a good agreement between the estimated effective radius and the real value despite using Hertz contact in the presence of friction. Future work will solve the existing limitations of the sensor and extend the application of the sensor to robotic manipulation tasks.

REFERENCES

[1] N. Hogan, "Impedance control: An approach to manipulation: Part i—theory," *Journal of dynamic systems, measurement, and control*, vol. 107, no. 1, pp. 1–7, 1985.

[2] A. Bicchi, J. K. Salisbury, and D. L. Brock, "Contact sensing from force measurements," *The International Journal of Robotics Research*, vol. 12, no. 3, pp. 249–262, 1993.

[3] C. Hudin, S. Panëels, and S. Strachan, "Intact: Instant interaction with 3d printed objects," in *Proceedings of the 2016 CHI Conference Extended Abstracts on Human Factors in Computing Systems*. ACM, 2016, pp. 2719–2725.

[4] T. J. Prescott, M. E. Diamond, and A. M. Wing, "Active touch sensing," 2011.

[5] M. Wiertlewski, J. Lozada, and V. Hayward, "The spatial spectrum of tangential skin displacement can encode tactual texture," *IEEE Transactions on Robotics*, vol. 27, no. 3, pp. 461–472, 2011.

[6] A. M. Kappers, "Human perception of shape from touch," *Philosophical Transactions of the Royal Society B: Biological Sciences*, vol. 366, no. 1581, pp. 3106–3114, 2011.

[7] M. A. Srinivasan and R. H. LaMotte, "Tactual discrimination of softness," *Journal of neurophysiology*, vol. 73, no. 1, pp. 88–101, 1995.

[8] K. Fujita and H. Ohmori, "A new softness display interface by dynamic fingertip contact area control," in *5th World Multiconference on Systemics, Cybernetics and Informatics*, 2001, pp. 78–82.

[9] J. Platkiewicz, H. Lipson, and V. Hayward, "Haptic edge detection through shear," *Scientific reports*, vol. 6, p. 23551, 2016.

[10] A. Goodwin, K. John, and A. Marceglia, "Tactile discrimination of curvature by humans using only cutaneous information from the fingerpads," *Experimental brain research*, vol. 86, no. 3, pp. 663–672, 1991.

[11] I. Birznieks, P. Jenmalm, A. W. Goodwin, and R. S. Johansson, "Encoding of direction of fingertip forces by human tactile afferents," *Journal of Neuroscience*, vol. 21, no. 20, pp. 8222–8237, 2001.

[12] R. S. Johansson and J. R. Flanagan, "Coding and use of tactile signals from the fingertips in object manipulation tasks," *Nature Reviews Neuroscience*, vol. 10, no. 5, pp. 345–359, 2009.

[13] R. S. Dahiya, G. Metta, M. Valle, and G. Sandini, "Tactile sensing—from humans to humanoids," *IEEE transactions on robotics*, vol. 26, no. 1, pp. 1–20, 2009.

[14] K. Sato, K. Kamiyama, N. Kawakami, and S. Tachi, "Finger-shaped gelforce: sensor for measuring surface traction fields for robotic hand," *IEEE Transactions on Haptics*, vol. 3, no. 1, pp. 37–47, 2009.

[15] D. Ma, E. Donlon, S. Dong, and A. Rodriguez, "Dense tactile force estimation using gelslim and inverse fem," in *2019 International Conference on Robotics and Automation (ICRA)*. IEEE, 2019, pp. 5418–5424.

[16] X. Lin and M. Wiertlewski, "Sensing the frictional state of a robotic skin via subtractive color mixing," *IEEE Robotics and Automation Letters*, vol. 4, no. 3, pp. 2386–2392, 2019.

[17] N. J. Ferrier and R. W. Brockett, "Reconstructing the shape of a deformable membrane from image data," *The International Journal of Robotics Research*, vol. 19, no. 9, pp. 795–816, 2000.

[18] Z. Kappassov, D. Baimukashev, Z. Kuanyshuly, Y. Massalin, A. Urazbayev, and H. A. Varol, "Color-coded fiber-optic tactile sensor for an elastomeric robot skin," in *2019 International Conference on Robotics and Automation (ICRA)*. IEEE, 2019, pp. 2146–2152.

[19] B. Ward-Cherrier, N. Pestell, L. Cramphorn, B. Winstone, M. E. Giannaccini, J. Rossiter, and N. F. Lepora, "The tactip family: Soft optical tactile sensors with 3d-printed biomimetic morphologies," *Soft robotics*, vol. 5, no. 2, pp. 216–227, 2018.

[20] W. Yuan, R. Li, M. A. Srinivasan, and E. H. Adelson, "Measurement of shear and slip with a gelsight tactile sensor," in *2015 IEEE International Conference on Robotics and Automation (ICRA)*. IEEE, 2015, pp. 304–311.

[21] T. Sakuma, F. Von Drigalski, M. Ding, J. Takamatsu, and T. Ogasawara, "A universal gripper using optical sensing to acquire tactile information and membrane deformation," in *2018 IEEE/RSJ International Conference on Intelligent Robots and Systems (IROS)*. IEEE, 2018, pp. 1–9.

[22] A. Schmitz, M. Maggiali, M. Randazzo, L. Natale, and G. Metta, "A prototype fingertip with high spatial resolution pressure sensing for the robot icub," in *Humanoids 2008-8th IEEE-RAS International Conference on Humanoid Robots*. IEEE, 2008, pp. 423–428.

[23] M. Shimojo, "Mechanical filtering effect of elastic cover for tactile sensor," *IEEE Transactions on Robotics and Automation*, vol. 13, no. 1, pp. 128–132, 1997.

[24] R. S. Fearing and T. O. Binford, "Using a cylindrical tactile sensor for determining curvature," in *Proceedings. 1988 IEEE International Conference on Robotics and Automation*. IEEE, 1988, pp. 765–771.

[25] A. M. Okamura and M. R. Cutkosky, "Feature detection for haptic exploration with robotic fingers," *The International Journal of Robotics Research*, vol. 20, no. 12, pp. 925–938, 2001.

[26] J. N. Israelachvili, *Intermolecular and surface forces*. Academic press, 2015.

[27] K. L. Johnson, *Contact mechanics*. Cambridge university press, 1987.

[28] T. Maeno, T. Kawamura, and S.-C. Cheng, "Friction estimation by pressing an elastic finger-shaped sensor against a surface," *IEEE Transactions on Robotics and Automation*, vol. 20, no. 2, pp. 222–228, 2004.

[29] J. Monnoyer, E. Diaz, C. Bourdin, and M. Wiertlewski, "Perception of ultrasonic switches involves large discontinuity of the mechanical impedance," *IEEE transactions on haptics*, vol. 11, no. 4, pp. 579–589, 2018.